Appeared, *Proceedings, 17th Intl. Conf. on Offshore Mechanics and Arctic Engineering* Lisbon, 1998
Under review, *Journal of OMAE,* ASME.

Reliability-Based Prediction of Design Loads and Responses for Floating Ocean Structures

Steven R. Winterstein
Civil and Environmental Engineering Department
Stanford University
Stanford, CA 94305-4020

Knut Engebretsen
Aker Engineering
Oslo, NORWAY
(Visiting Scholar, Stanford University)

Abstract

Procedures are described to define design loads and responses of ocean structures. While these methods can be used for both fixed and floating structures, this paper focuses on applications to floating structures; specifically, extreme motions of both a tension-leg platform (TLP) and a spar buoy, and the extreme tether tension of a TLP. To capture the important sensitivity of floating structures to wave period as well as height, joint contours of significant wave height and peak spectral period are derived. Because these contours are structure-independent, they provide a useful means to specify important combinations of environmental parameters for design and wave tank experiments. New methods are also developed to predict the effect of response variability. These quantify both the response variability in a given seastate, and the background variability in the median response (over all seastates). The result suggests that slow drift motions may provide a particular modelling challenge: they combine relatively large response variability with rather low background variability levels, the latter due to the limiting steepness behavior of their critical seastates.

Introduction

In various applications, reliability concepts have led to the formulation of load and resistance-factor design (LRFD) procedures. One such application appears in the recent LRFD guidelines for fixed offshore structures, developed by the American Petroleum Institute (API, 1993). In general, such procedures scale nominal loads and resistances, L_{nom} and R_{nom}, by separate load and resistance factors:

$$\phi_R R_{nom} \geq \gamma_L L_{nom} \tag{1}$$

Of course, for any single case—i.e., a specific structural limit state in a specific random environment—it is equivalent to specify only the ratio ϕ_R/γ_L, which provides a single multiplier on the nominal safety factor R_{nom}/L_{nom}. More generally, use of the separate factors γ_L and ϕ_R in Eq. 1 aims to achieve more uniform reliability over multiple cases, in which loads may show different degrees of variability with respect to resistances. Similarly, the design load $L_{des}=\gamma_L L_{nom}$ may be split further into separate contributions which show different levels of variability, and hence are assigned different load factors. Examples of this include the separate dead and live

load factors in various building codes, or the separate factors recently suggested for static, wave-frequency, and slow-drift loads on floating structures (Banon et al, 1994). (Note that while we refer to "design loads" here, following common practice these design levels may generally be cast in terms of loads, load effects, or response levels.)

Here we consider appropriate design levels of load and responses for floating structures. Due to their dynamic behavior, it is necessary to model the input wave elevation not merely as a single severe wave cycle, but rather as a set of irregular, random process realizations over a sequence of stationary, 3-hour "seastates". Within each seastate, the wave elevation $\eta(t)$ is commonly parameterized by its significant wave height, H_s=$4\sigma_\eta$, and its peak spectral period, T_p. (Here σ_η denotes the standard deviation of $\eta(t)$). During a seastate with given H_s and T_p, the maximum response (offset, tether tension, etc.) is then expressed as

$$X = \hat{X}(H_s, T_p) \cdot \epsilon \qquad (2)$$

in which $\hat{X}(H_s, T_p)$ denotes the median value of the maximum response given H_s and T_p, while ϵ is a unit-median random variable which reflects the scatter in maximum response due to different input wave histories, $\eta(t)$, with the same gross statistics, H_s and T_p.

In offshore design practice it is common to associate the nominal load L_{nom} in some way with a return period of 100 years. Various definitions of L_{nom} may be considered:

Case 1: $L_{nom,1}$=$\hat{X}(H_{100}, \hat{T}_p|H_{100})$, the representative load associated with the 100-year significant wave height, H_{100}, and typical period $\hat{T}_p|H_{100}$ (e.g., median value given H_{100}). Uncertainty is thus neglected both in T_p and in the load given H_s (i.e., ϵ is set to 1 in Eq. 2).

Case 2: $L_{nom,2}$=$\hat{X}_{100}$, the 100-year value of the median load, including randomness in both H_s and T_p. Uncertainty is now neglected only in the load given H_s and T_p (again, ϵ=1 is assumed).

Case 3: $L_{nom,3}$=X_{100}, the "true" 100-year load/response. This includes uncertainty in both H_s and T_p, and in the load given H_s and T_p. This is then a problem involving three random variables: H_s, T_p, and ϵ.

It is clear that by more fully including complete uncertainty, these loads increase in order; i.e., $L_{nom,1} \leq L_{nom,2} \leq L_{nom,3}$. In principle, any choice of nominal load L_{nom} can be used if associated with a consistent load factor. This would suggest higher γ_L with $L_{nom,2}$ than with $L_{nom,3}$, and still higher γ_L associated with $L_{nom,1}$. The main drawback is that the ratio, $L_{nom,3}/L_{nom,1}$, will generally depend on both the structure and the environment. Because a single factor applied to $L_{nom,1}$ cannot reflect this dependence, it must lead to a range of reliability levels. The virtue of $L_{nom,3}$ is that it carries the most case-specific information on both structure and site. Its corresponding drawback is that it is the most difficult to calculate.

We show here some simple methods to perform these more detailed load calculations, with applications to floating structures (e.g., slow drift of TLP and spar platforms, ringing response of TLPs). In particular, we describe in some detail how 100-year H_s–T_p design contours can be created to directly estimate $L_{nom,2}$. Simple corrections are then sought to estimate the actual 100-year load, $L_{nom,3}$. The use of design H_s–T_p contours is currently under consideration in various offshore design applications; e.g., the new NORSOK guidelines governing load calculations for structures along the Norwegian continental shelf. One goal of this paper is to aid these efforts, providing technical documentation and support for design-contour methods.

Design Contours

Contours 1: Their Goal

A virtue of the simplest nominal load definition, $L_{nom,1}$, is that it requires only a single (H_s, T_p) combination: the 100-year H_s level and an associated period, e.g. the median $\hat{T}_P|H_{100}$.

A 100-year contour, $(H_s, T_p)_{100}$, seeks to generalize this concept to two dimensions; namely, to specify all (H_s, T_p) pairs that are candidates, by virtue of their relative rareness, to produce the 100-year level of *any* load or response quantity. For example, the 100-year value of the median response, $\hat{X}(H_s, T_p)$ above, would be estimated as

$$\hat{X}_{100} = \max \hat{X} \text{ along } (H_s, T_p)_{100} \text{ contour} \quad (3)$$

New methods to generate such contours have been recently proposed, by introducing the Inverse FORM method (Winterstein et al, 1993, Ude and Winterstein, 1996). This method can give contours for any number of variables, correlated or not, and for any return period T of interest. They require knowledge only of the joint probability distribution of all governing variables (here, of H_s and T_p). These contours also show internal consistency; for example, the two-dimensional contour $(H_s, T_p)_{100}$ includes the original checking point $(H_{100}, \hat{T}_p|H_{100})$, which remains the critical seastate for structures that are insensitive to period T_p.

Contours 2: Their Construction

While the theoretical basis underlying these contours requires knowledge of FORM (first-order reliability methods), they may be constructed directly without such knowledge. We therefore seek to describe their construction in some detail here. It is useful to consider first a completely artificial—but easily generalized—situation, in which all random variables have standard normal distributions, and are statistically independent. (These are commonly denoted U_1, U_2, ..., and the resulting standardized problem is sometimes said to be cast in "U–space.") Any return period T can then be related to a corresponding fractile, β, of a normal variable. For example, because there are 365×8=2920 3-hour seastates per year, the return period T=100 years implies a failure probability of p_f=1/(100 × 2920) or 3.43×10^{-6} per seastate. Setting $P[U_i > \beta]$=1 − $\Phi(\beta)$ to this p_f value yields β=4.50.

For example, if there is only one normal variable U_1, the mean return period T=100 years requires that the limit state be located at U_1=β=4.50 standard deviations away from the mean. In a two-dimensional case, the 100-year "U-space" contour is simply the locus of all points at distance β=4.50 away from the mean value U_1=U_2=0. In general, this leads to a circle with radius β_T, a function of the desired return period T:

$$|u|^2 = u_1^2 + u_2^2 = \beta_T^2 \quad (4)$$

For T=100, β_T=4.50 as discussed above. Table 1 shows how β_T varies over a range of return periods T. Finally, the cumulative distributions $F_{H_s}(h_s)$ and $F_{T_p|H_s}(t_p|h_s)$, of H_s and of T_p given H_s, are used to transform each point on the circle $|u|$=β into corresponding h_s–t_p values:

$$\Phi(u_1) = F_{H_S}(h_s)\,; \quad \Phi(u_2) = F_{T_P|H_S}(t_p|h_s) \quad (5)$$

Return Period T [yrs]	Failure Probability p_f [per 3-hr seastate]	Limit State Distance β_T=$\Phi^{-1}(1-p_f)$
30	1.14×10^{-5}	4.24
100	3.43×10^{-6}	4.50
300	1.14×10^{-6}	4.73
1000	3.43×10^{-7}	4.97
3000	1.14×10^{-7}	5.17
10000	3.43×10^{-8}	5.40

Table 1: Relation between design return period, T, and limit state distance, β_T.

Numerical Results

Figure 1 shows resulting 100- and 10000-year contours for a Northern North Sea site with documented H_s–T_p statistics (Haver and Nyhus, 1986). These were constructed by applying Eq. 5 to U-space circles, with radii β_{100}=4.50 and β_{10000}=5.40 (Table 1). The largest H_s values of these contours correspond to 100- and 10000-year marginal levels: H_{100}=14.5m and H_{10000}=17.7m.

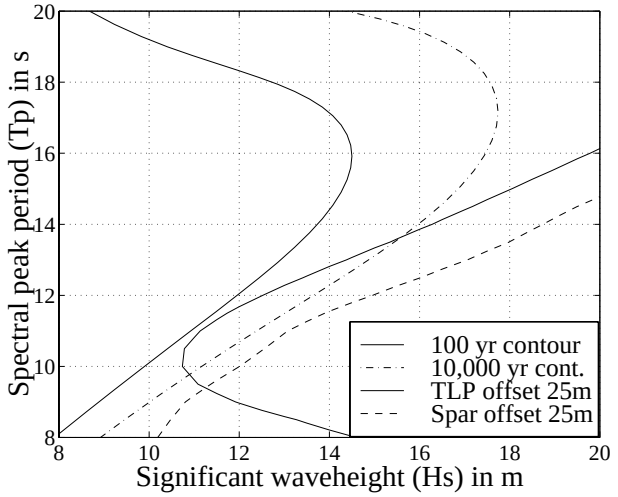

Figure 1: H_s–T_p contours and TLP/spar iso-response lines.

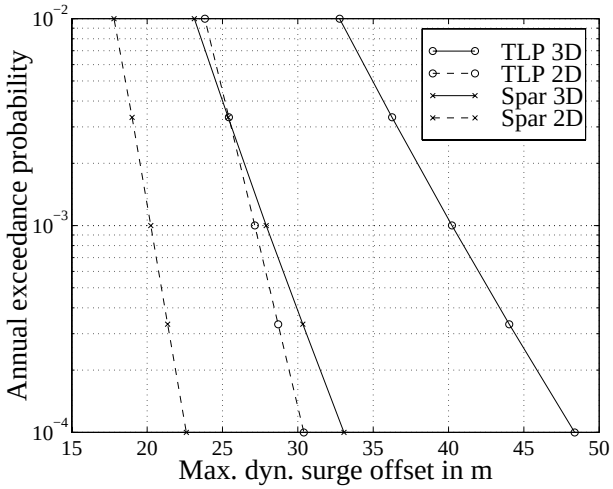

Figure 2: Annual exceedance probabilities of various surge offsets.

Figure 1 also shows iso-response lines for the surge offset of both a TLP and a spar buoy platform. In particular, all (H_s–T_p) pairs are shown which produce a median extreme of $\hat{X}$=25m of dynamic offset in head seas. (To standardize results and aid comparisons, we report in all cases the dynamic extreme, removing structure-specific mean offset levels.) These response statistics have been found from the post-processing analysis routine `TFPOP` (Ude et al, 1995). This uses the linear and quadratic force transfer functions, and added mass and damping, computed from diffraction/radiation analysis (Kim and Yue, 1988; WAMIT, 1995). `TFPOP` then constructs corresponding linear and quadratic transfer functions to the response $x(t)$. (In general it can include forces/moments in all 6DOF, and analyze any response quantity such as motion, acceleration, tether tension, etc.) A convenient model of nonlinear random vibration, the "Hermite" model, is then used to predict various fractiles of extremes from the first four moments of $x(t)$—the mean μ, standard deviation σ, skewness α_3, and kurtosis α_4—and its average crossing rate f_0. This model has been verified through simulation for both TLPs and semi-submersible platforms (Winterstein et al, 1994) and for a spar buoy model (Winterstein et al, 1995).

Note that the TLP studied here has a symmetric hull with four columns, with diameters d=25m and center-to-center spacing of L=76m. This column spacing dictates that for fixed H_s, a seastate with $T_p \approx$ 10s will cause extreme slow-drift response. The TLP iso-response line in Figure 1 confirms this critical-period effect. In contrast, the spar buoy hull is a single cylinder with draft h=198m, diameter d=42.7m, and a center well to protect drilling and production risers. Unlike the multi-column TLP, the spar's geometry does not produce any single critical wave period/length. Instead, the spar response shows a general increasing trend with the seastate steepness (i.e., increasing H_s or decreasing T_p). This supports the possibility of various critical (H_s, T_p) locations—depending on the precise spar buoy dimensions and its modelling assumptions—and hence the need to specify a full two-dimensional (H_s, T_p) contour as in Figure 1.

Figure 2 shows the resulting distribution of the actual maximum offset, X, and the median maximum offset, $\hat{X}$, for both the TLP and the spar. For example, its "2D" (median max) results are found by searching two-dimensional (H_s, T_p) contours, with appropriate return periods, to find the maximum $\hat{X}$ value. As Figure 1 shows, the 100-year value $\hat{X}_{100}$ for the TLP should be

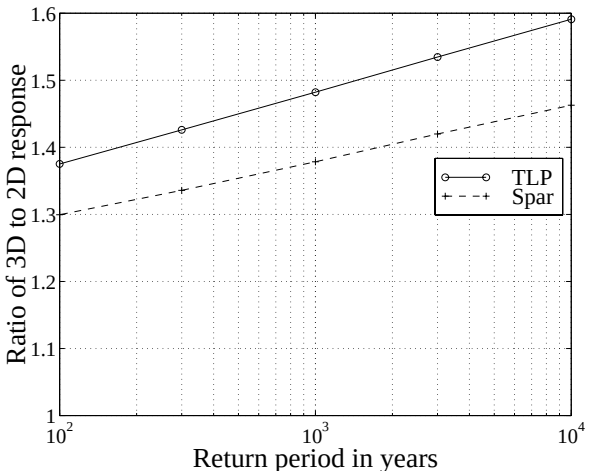

Figure 3: Contour-based estimates of $R{=}X/\hat{X}$, in which X=actual maximum response; $\hat{X}$=median maximum response.

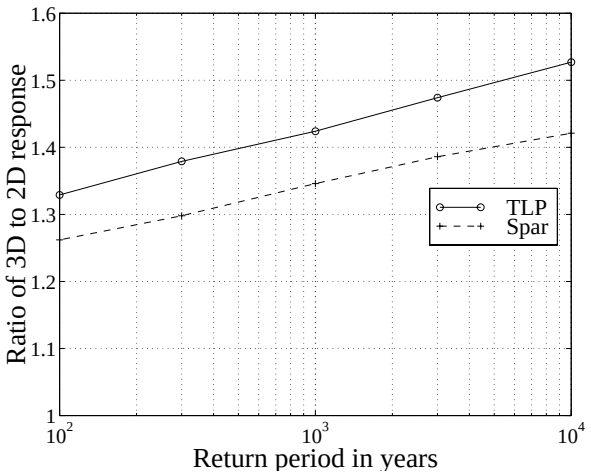

Figure 4: Simulation-based estimates of $R{=}X/\hat{X}$, in which X=actual maximum response; $\hat{X}$=median maximum response.

slightly less than 25m (in fact $\hat{X}_{100}$=23.8m), while even $\hat{X}_{10000}$ for the spar should be less than 25m (actually $\hat{X}_{10000}$=22.6m). The "3D" results shown for the actual maximum X were found by searching an analogous three-dimensional H_s–T_p–ϵ contour. Inclusion of this response variability term, ϵ from Eq. 2, is shown to yield larger extremes: for the spar the 100-year offset increases from $\hat{X}_{100}$=17.8m to X_{100}=23.1m, and for the TLP from $\hat{X}_{100}$=23.8m to X_{100}=32.8m.

For a given return period T, the TLP and spar will typically not show similar values of $\hat{X}_T$ or X_T in absolute numerical terms. One may hope, however, that both extreme offset cases show similar values of the *ratio* $R_T{=}X_T/\hat{X}_T$. If so, this could suggest simple correction factors, R_T, to adjust the simpler 2D results for $\hat{X}_T$. Unfortunately, Figure 3 shows that this ratio R_T (on its vertical axis) is significantly larger for the TLP: R_{100}=1.38 (TLP) versus R_{100}=1.30 (spar). Note also the relatively large R_T values in both cases: if one begins with a nominal load $L_{nom,2}{=}\hat{X}_{100}$ as previously defined, a common load factor value γ_L=1.3 barely serves to return $L_{nom,3}{=}X_{100}$, with no extra conservatism either to achieve rarer exceedances or to cover other uncertainty (e.g., in analytical load predictions). We therefore devote most of our remaining efforts to explain this large value of the inflation factor, $R_T{=}X_T/\hat{X}_T$, and simple procedures to predict it.

1: FORM vs Simulation

A principal assumption of FORM, and hence of Inverse-FORM and its resulting contours, is that the true limit state function is replaced by a straight line/plane. (Strictly, this linearization is performed on the standardized problem; i.e., when the limit state is viewed "in U–space.") It may be expected, in view of the curvature Figure 1 shows for the TLP limit state, that FORM may be especially conservative in this case. Figure 4 shows, however, that the FORM approximation is not the main source of difference between the R_T ratios for the two structures. This figure recalculates R_T based not on FORM approximations but rather on numerous simulations, which yield unbiased estimates for any limit-state function. (For efficiency these simulations use importance sampling, with a sampling density centered at the critical seastate found by the design-contour search.) Figure 4 shows that the ratio $R_T{=}X_T/\hat{X}_T$ is slightly lower than that predicted by FORM/Inverse-FORM (Figure 3). The difference is not large, however, and the

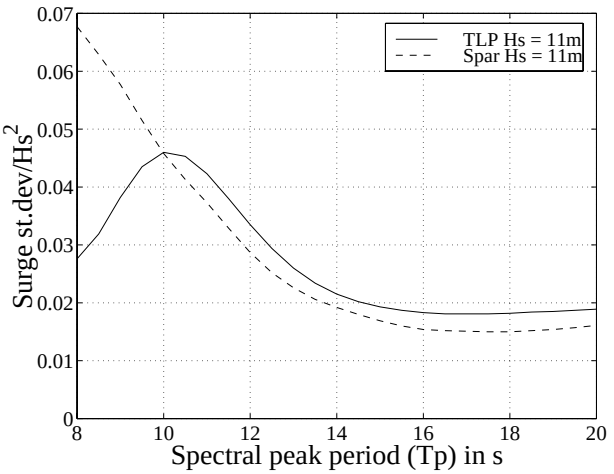

Figure 5: Standard deviation σ of surge response, normalized by H_s^2.

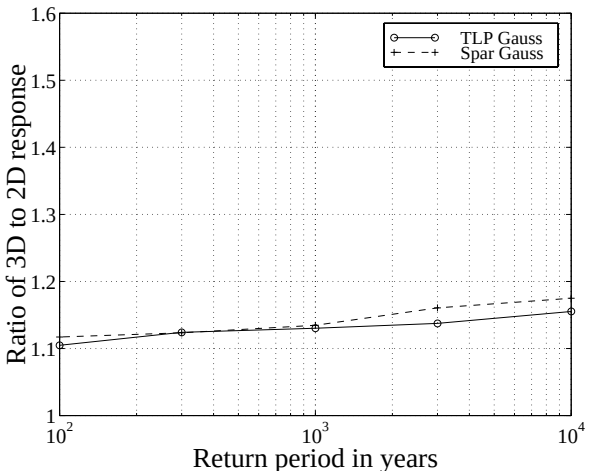

Figure 6: Gaussian-based estimate of $R{=}X/\hat{X}$ between X=actual maximum response; $\hat{X}$=median maximum response.

systematic difference between the TLP and spar cases remains.

2: Different RMS Behavior

As Figure 1 reveals, the multi-column TLP shows markedly different behavior when viewed versus the peak period T_p. At a most fundamental level, this manifests itself statistically through different trends in the standard deviation (RMS), σ, of the surge response. (Recall that the mean surge response has been removed in both cases.) Figure 5 shows the behavior of σ/H_s^2 versus T_p; because quadratic load effects dominate, this ratio is relatively insensitive to H_s (Engebretsen and Winterstein, 1998.) Again, only the TLP shows the critical period $T_p \approx 10$s.

To isolate this effect, we construct Gaussian models of both the spar and TLP surge response, using these RMS values and setting higher response moments to their Gaussian values: $\alpha_3{=}0$, $\alpha_4{=}3$. The resulting ratio $R_T{=}X_T/\hat{X}_T$ is shown in Figure 6 to reduce dramatically: R_{100} is roughly 1.1, and even R_{10000} remains less than 1.2. Moreover, differences between the TLP and spar have become negligible. This implies that the large, case-specific R_T values in Figure 3 are *not* due to the difference in RMS behavior in Figure 5. (Indeed, for most cases of interest here the critical seastate has period T_p of at least 10s, above which the two rms values behave relatively similarly.)

3: Different Higher-Moment Behavior

Finally, we are led to consider the higher moments, and hence non-Gaussian behavior, of the surge offset response for the two structures. Figure 7 shows that the the two structures show similar response skewness values over the important range of seastate periods (roughly, T_p from 10–15s). Figure 8, however, shows the TLP response to have significantly larger kurtosis: α_4 of nearly 4.5 when $T_p{=}10$s, compared with roughly 3.5 for the spar. It is this effect that causes the larger R_T ratio for the TLP: due to its multi-column geometry, in the critical $T_p{=}10$s seastate the TLP platform shows systematically larger extreme offsets than the spar, although the two have similar rms response levels. These results show the need for an appropriate non-Gaussian response model, lest one neglect this difference entirely as in Figure 6. (Note an important caveat: all result here assume linear damping. The absolute numerical values are likely to change in the presence of wave drift damping, which tends to "clip" extreme slow-drift motions. The present cases, however, are particularly well-suited to test the limits of the approximate models of response variability in the next section.)

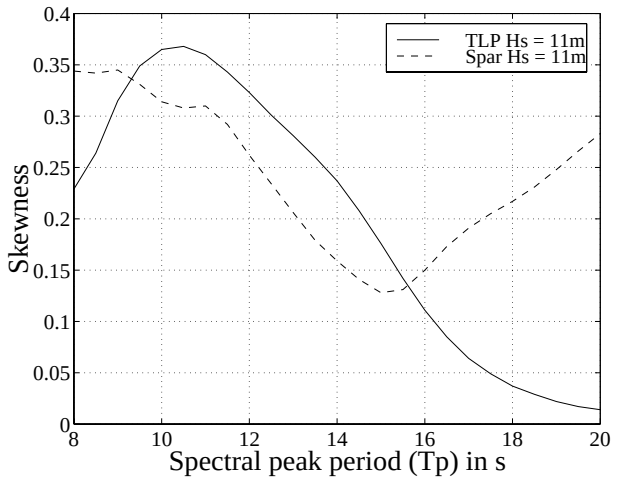

Figure 7: Skewness α_3 of surge response, TLP and spar.

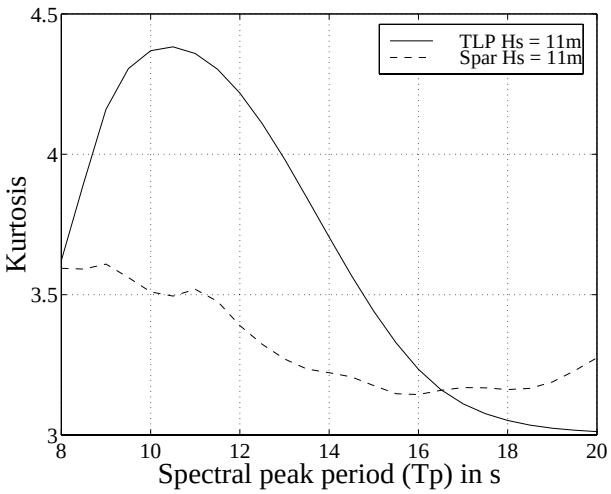

Figure 8: Kurtosis α_4 of surge response, TLP and spar.

Correcting for Response Variability

In view of the foregoing results, we consider and evaluate simple methods to correct the median maximum, $\hat{X}_{100}$ as in Eq. 3, to account for response variability. One approach, used for example by Statoil since the mid-1980s (Haver et al, 1998), uses Eq. 3 with an inflated return period. Recently, Inverse-FORM has been used to derive an expression for the inflated contour radius: the original radius β_T should be increased by $1/\sqrt{1-\alpha_\epsilon^2}$, in which α_ϵ^2 is the relative response variability due to ϵ (Winterstein et al, 1993).

More recent trends favor reporting the H_s–T_p contour with its actual return period, and seeking other means to inflate the response from its median level. One proposal is to apply Eq. 3 not with the median response, but rather with a higher response fractile p:

$$X_{100} = \max\, X_p \text{ along } (H_s, T_p)_{100} \text{ contour} \quad (6)$$

The fractile level p=.85–.90 has been recently suggested (Haver et al, 1998); we shall show results here for p=.90 only. (Again, FORM provides a theoretically "optimal" but case-specific choice of p, corresponding to the standard normal fractile $U_\epsilon^+ = [1-\sqrt{1-\alpha_\epsilon^2}]\beta_T/\alpha_\epsilon$; Madsen, 1988; Bjerager, 1990.)

Figures 9 and 10 show the use of Eq. 6, with the p=90% fractile response, for the TLP and spar cases respectively. Results are rather accurate, particularly at the T=100 year level for which the method has been proposed (predicted R_{100}=1.29 and 1.25 for the TLP and spar, compared with the actual values R_{100}=1.38 and 1.30.)

For longer return periods, however, use of the 90% fractile becomes increasingly non-conservative. These figures also show results from an approximate, locally-fit lognormal model of $\hat{X}$ and of ϵ. For example, a lognormal model of $\hat{X}$ implies that $\hat{X}_T = \exp[\mu_{\ln \hat{X}} + \sigma_{\ln \hat{X}}\beta_T]$. Fitting this to two return period values, $\hat{X}_{T_1}$ and $\hat{X}_{T_2}$, the implied standard deviation is

$$\sigma_{\ln \hat{X}} = \frac{\ln(\hat{X}_{T_1}/\hat{X}_{T_2})}{(\beta_{T_1} - \beta_{T_2})} \quad (7)$$

The return periods T_1 and T_2 should be chosen in the vicinity of the desired return period (and slightly less); e.g., for the 1000-year response one may choose to fit Eq. 7 at T_1=1000 and T_2=300 years. (Table 1 gives corresponding β_T values.) The resulting $\sigma_{\ln \hat{X}}$ value reflects the uncertainty in the median response, due to seastate variability. The corresponding $\sigma_{\ln \epsilon}$ can be estimated from two fractiles of the *actual* response in the critical seastate (e.g., the predicted critical 1000-year seastate found from a 2D-contour search).

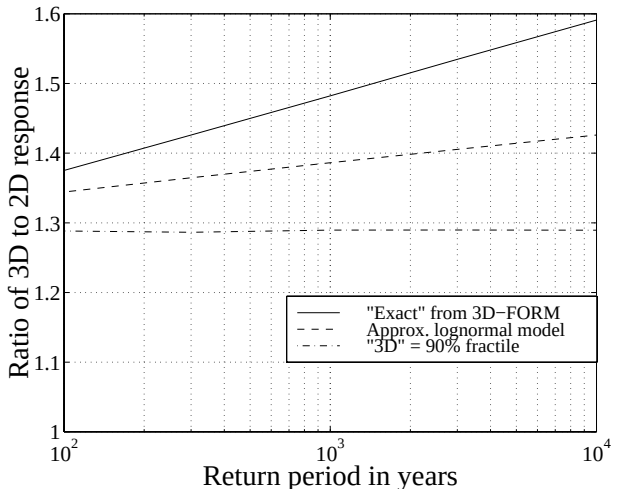

Figure 9: Estimates of $R{=}X/\hat{X}$ for TLP: comparing full (3D-FORM) analysis with (a) approximate lognormal model; (b) 90%-fractile response.

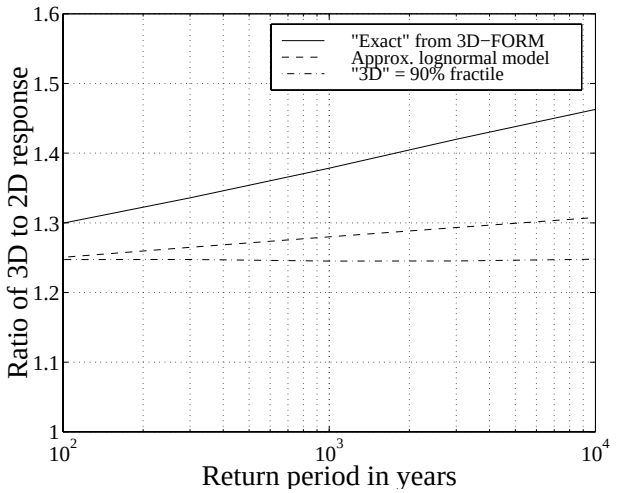

Figure 10: Estimates of $R{=}X/\hat{X}$ for spar: comparing full (3D-FORM) analysis with (a) approximate lognormal model; (b) 90%-fractile response.

To be somewhat consistent with the previous approach, we fit here to the 50% and 90% response fractiles:

$$\sigma_{\ln \epsilon} = \frac{\ln(\epsilon_{.90}/\epsilon_{.50})}{1.28} \qquad (8)$$

Again, $\epsilon_{.90}/\epsilon_{.50}$ denotes simply the ratio of the 90% to 50% response fractiles in the critical seastate of interest.

Notably, $\sigma_{\ln \hat{X}}$ is found here to be relatively stable, remaining at roughly 0.27 for both the TLP and spar offsets across a range of return periods T_1 and T_2. As Table 2 reveals, however, the response variability $\sigma_{\ln \epsilon}$ is somewhat greater for the TLP (0.20 vs. 0.17 for the spar). Finally, Figures 9 and 10 show the resulting correction factor R_T based on these lognormal models:

$$R_T = \frac{X_T}{\hat{X}_T} = \exp[(\sigma_{\ln X} - \sigma_{\ln \hat{X}})\beta_T] \qquad (9)$$

in which $\sigma^2_{\ln X}{=}\sigma^2_{\ln \hat{X}} + \sigma^2_{\ln \epsilon}$. This estimate of R_T is found somewhat more accurate than the 90%-fractile result over a range of return periods, increasing with T through varying β_T (again as in Table 1). In general it reveals the dependence of R_T on the value of response variability, $\sigma_{\ln \epsilon}$, *relative* to the "background" variability $\sigma_{\ln \hat{X}}$ in median response due to seastate variability. In this case an apparently small difference in $\sigma_{\ln \epsilon}$, 0.20 vs 0.17, has a significant effect because the background variability, $\sigma_{\ln \hat{X}}$, is also rather low. (This reflects the fairly narrow distribution of seastates in the H_s–T_p scattergram in the steep, T_p=10s region.)

Case	$\sigma_{\ln \hat{X}}$	$\sigma_{\ln \epsilon}$
TLP surge	0.27	0.20
Spar surge	0.27	0.17
TLP tension	0.49	0.19

Table 2: Variability in median maximum, $\hat{X}$, and in response variability term ϵ.

TLP Ringing Response

As a final example, we consider the tension response of the bow tether of the Heidrun TLP in diagonal seas. Model tests of this TLP have provided the most notable example of transient resonant response episodes, commonly denoted "ringing" (e.g., Davies et al, 1994). Due to the lack of concensus regarding an analytical ringing model, we base our results here directly on response surfaces fit to the tether tension moments and cycle rate, (μ, σ, α_3, α_4, f_0), observed across

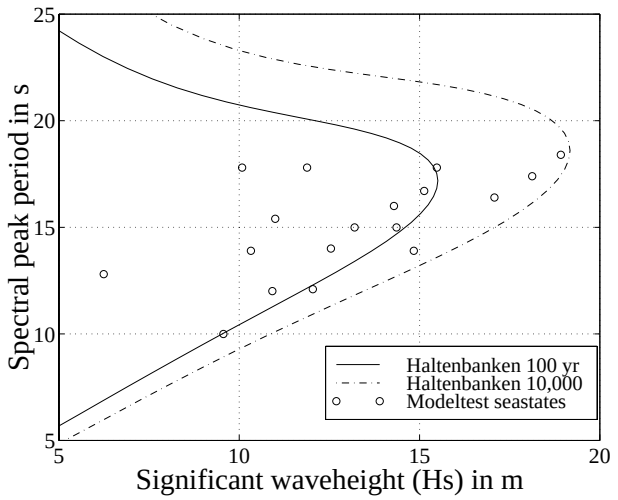

Figure 11: Haltenbanken H_s–T_p contours and model test seastates.

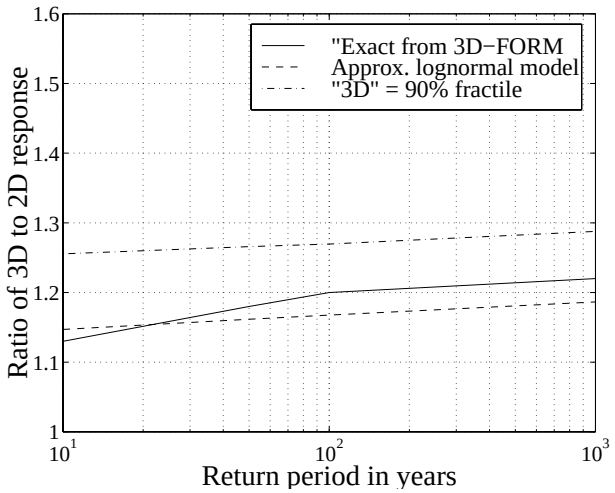

Figure 12: Estimates of $R{=}X/\hat{X}$ for TLP tether tension: comparing full (3D-FORM) analysis with (a) approximate lognormal model; (b) 90%-fractile response.

various H_s–T_p model tests. A rather extensive model test series is available; tested (H_s, T_p) values are shown as points in Figure 11. This figure also shows 100- and 10000-year contours for Haltenbanken, the North Sea site where Heidrun is located.

Figure 12 shows corresponding correction ratios $R_T{=}X_T/\hat{X}_T$, relating the actual and median extreme, now for return periods $T{=}10$—1000 years (there is a scarcity of model test data at longer return periods). In view of the known nonlinearity of ringing, it is perhaps surprising to find notably smaller correction ratios R_T for ringing than for the slow drift cases in Figure 3. (In fact, in this case the 90% fractile estimate from Eq. 6 is rather conservative.) The explanation of this is revealed by again estimating the levels of both the response variability, $\sigma_{\ln \epsilon}$, and the background variability $\sigma_{\ln \hat{X}}$ as in Eqs. 7–8. Table 2 reveals that the ringing response variability is comparable to that of slow drift ($\sigma_{\ln \epsilon}{=}0.19$); the major difference is that this variability is now quite small compared with the background level, $\sigma_{\ln \hat{X}}{=}0.49$. This higher background level reflects that the critical ringing seastate is now governed by extreme H_s events, which show broader variability than the steeper, small T_p seastates found critical for slow drift. Thus, the slow drift case may be expected to be one of the most challenging to model response variability: it combines relatively large response variability with rather low background variability levels (due to the limiting steepness behavior of seastates).

Summary and Conclusions

We have shown here how design seastate contours can be constructed, and used to estimate design loads and responses of ocean structures. These contours permit decoupling of the environmental specification from the structural concept. As a result, these contours can suggest robust criteria for structural code checks and standards, as well as for design of wave tank experiments.

In cases where the extreme response X is well-approximated by its median value, $\hat{X}$, the T-year response can be found directly by searching an appropriate T-year H_s–T_p contour (e.g., Figure 1). For extreme offsets of floating structures, however, neglecting response variability may lead to significant non-conservatism. For example, Figure 3 shows the actual 100-year response to be roughly 1.3–1.4 times the median 100-year value $\hat{X}_{100}$, with larger multipliers in the case of a TLP

than of a spar buoy. These large, case-specific multipliers are found not to be preserved if a Gaussian model of surge motion is instead used (Figure 6). This reflects the need to preserve the non-Gaussian response aspects in estimating extremes; in particular, the larger kurtosis shown by the TLP in T_p=10s seastates (Figure 8), due to the spacing between its multiple columns.

New methods have also been developed to predict the effect of response variability. These quantify both the response variability in a given seastate (Eq. 8), and the background variability in the median response over all seastates (Eq. 7). The resulting lognormal approximation in Eq. 9 has been found to be reasonably accurate over the various cases studied (Figures 9–10 and Figure 12). They provide a useful alternative to a complete long-term reliability analysis, which explicitly retains randomness in H_s, T_p, and response given H_s and T_p.

Acknowledgements

Both authors gratefully acknowledge Aker Engineering, for supporting the second author's stay as a Visiting Scholar within the RMS program at Stanford University. Support for the first author has been provided by the National Science Foundation through the Offshore Technology Research Center (Grant CDR-8721512), and by the Office of Naval Research (Grant N0014-9610641). Statoil is also gratefully acknowledged for supplying model test data for the Heidrun TLP.

References

API, RP2A-LRFD (1993). *Recommended practice for planning, designing and constructing fixed offshore platforms—load and resistance factor design,* 1st edition, American Petroleum Institute.

Banon, H., G.R. Toro, E.R. Jefferys and R.S. De (1994). Development of reliability-based global design equations for TLPs. *Proc., 13th Intl. Offshore Mech. Arctic Eng. Symp.,* ASME, **II**, 335–343.

Bjerager, P. (1990). Discussion: Omission sensitivity factors. *Struc. Safety*, **7**, 77–79.

Davies, K.B., S.J. Leverette and M.W. Spillane (1994). Ringing response of TLP and GBS platforms. *Proc., BOSS-94,* **2**, 569–585.

Engebretsen, K. and S.R. Winterstein (1998). *Probability-based design loads and responses of floating structures: extreme slow drift motion and tether tension,* Rept. RMS–30, Reliability of Marine Structures Program, Dept. of Civ. & Environ. Eng., Stanford University.

Haver, S. and K.A. Nyhus (1986). A wave climate description for long term response calculations. *Proc., 5th OMAE Symp.,* ASME, **IV**, 27–34.

Haver, S., G. Sagli and T.M. Gran (1998). Long term response analysis of fixed and floating structures. *Proc., Wave'98—Ocean Wave Kinematics, Dynamics and Loads on Structures,* International OTRC Symposium, Apr. 30–May 1, 1998, to appear.

Kim, M.H. and D.K.P. Yue (1988). The nonlinear sum-frequency wave excitation and response of a tension-leg platform. *Proceedings, BOSS'88,* Trondheim.

Madsen, H.O. (1988). Omission sensitivity factors. *Struc. Safety*, **5**, 35–45.

Ude, T.C. and S.R. Winterstein (1996). Ocean environment contours for structural response analysis and experiment design. *Proc., 7th Prob. Mech. Spec. Conf., ASCE,* Worcester.

Ude, T.C., S. Kumar and S.R. Winterstein (1995). *TFPOP 2.0: Stochastic response analysis of floating structures under wind, current, and second-order wave loads,* Rept. RMS–18, Reliability of Marine Structures Program, Dept. of Civ. Eng., Stanford University.

WAMIT, 4.0 (1995). *WAMIT: a radiation-diffraction panel program for wave-body interactions–user's manual,* Dept. of Ocean Eng., M.I.T.

Winterstein, S.R., S. Kumar, and G. Kleiven (1995). Environmental contours and extreme response of deep-water floating structures. *Proc., 10th Eng. Mech. Spec. Conf.,* ASCE, **2**, 1187–1190.

Winterstein, S.R., T.C. Ude and G. Kleiven

(1994). Springing and slow-drift responses: predicted extremes and fatigue vs. simulation. *Proc., BOSS-94,* **3**, Massachusetts Institute of Technology, 1–15.

Winterstein, S.R., T.C. Ude, C.A. Cornell, P. Bjerager and S. Haver (1993). Environmental parameters for extreme response: Inverse FORM with omission factors. *Proc., ICOSSAR-93,* Innsbruck.